



HAL
open science

The S218L familial hemiplegic migraine mutation promotes deinhibition of Ca(v)2.1 calcium channels during direct G-protein regulation.

Norbert Weiss, Alejandro Sandoval, Ricardo Felix, Arn van den Maagdenberg,
Michel de Waard

► To cite this version:

Norbert Weiss, Alejandro Sandoval, Ricardo Felix, Arn van den Maagdenberg, Michel de Waard. The S218L familial hemiplegic migraine mutation promotes deinhibition of Ca(v)2.1 calcium channels during direct G-protein regulation.: FHM-1 mutations promote G-protein deinhibition of Cav2.1 channels. *Pflügers Archiv European Journal of Physiology*, 2008, 457 (2), pp.315-26. 10.1007/s00424-008-0541-2 . inserm-00376518

HAL Id: inserm-00376518

<https://inserm.hal.science/inserm-00376518>

Submitted on 29 Oct 2009

HAL is a multi-disciplinary open access archive for the deposit and dissemination of scientific research documents, whether they are published or not. The documents may come from teaching and research institutions in France or abroad, or from public or private research centers.

L'archive ouverte pluridisciplinaire **HAL**, est destinée au dépôt et à la diffusion de documents scientifiques de niveau recherche, publiés ou non, émanant des établissements d'enseignement et de recherche français ou étrangers, des laboratoires publics ou privés.

The S218L familial hemiplegic migraine mutation promotes deinhibition of Ca_v2.1 calcium channels during direct G-protein regulation

Weiss Norbert¹, Sandoval Alejandro^{2,3}, Felix Ricardo², Van den Maagdenberg Arn^{4,5}, De Waard Michel^{1*}

¹GIN, Grenoble Institut des Neurosciences INSERM : U836, CEA, Université Joseph Fourier - Grenoble I, CHU Grenoble, UJF - Site Santé La Tronche BP 170 38042 Grenoble Cedex 9,FR

²Department of Cell Biology CINVESTAV-IPN, Avenida IPN #2508, Mexico City, CP 07300,MX

³School of Medicine FES Iztacala National Autonomous University of Mexico, Tlalnepantla,MX

⁴Department of Human Genetics Leiden University Medical Centre, P.O. Box 9600, 2300 RC Leiden,NL

⁵Department of Neurology Leiden University Medical Centre, P.O. Box 9600, 2300 RC Leiden,NL

* Correspondence should be addressed to: Michel De Waard <michel.dewaard@ujf-grenoble.fr>

Abstract

Familial hemiplegic migraine type 1 (FHM-1) is caused by mutations in CACNA1A; the gene encoding for the Ca_v2.1 subunit of voltage-gated calcium channels. Although various studies attempted to determine biophysical consequences of these mutations on channel activity, it remains unclear exactly how mutations can produce a FHM-1 phenotype. A lower activation threshold of mutated channels resulting in increased channel activity has been proposed. However, hyper-activity may also be caused by a reduction of the inhibitory pathway carried by G-protein coupled receptor activation. The aim of this study is to determine functional consequences of the FHM-1 S218L mutation on direct G-protein regulation of Ca_v2.1 channels. In HEK 293 cells, DAMGO activation of human μ -opioid receptors induced a 55% Ba²⁺ current inhibition through both wild-type and S218L mutant Ca_v2.1 channels. In contrast, this mutation considerably accelerates the kinetic of current deinhibition following channel activation by 1.7- to 2.3-fold depending on membrane potential values. Taken together, these data suggest that the S218L mutation does not affect G-proteins association onto channel in the closed state, but promotes its dissociation from the activated channel thereby decreasing the inhibitory G-protein pathway. Similar results were obtained with the R192Q FHM-1 mutation, although of lesser amplitude, which seems in line with the less severe associated clinical phenotype in patients. Functional consequences of FHM-1 mutations appear thus as the consequence of the alteration of both intrinsic biophysical properties and of the main inhibitory G-protein pathway of Ca_v2.1 channels. The present study furthers molecular insight in the physiopathology of FHM-1.

MESH Keywords Animals ; Calcium Channels ; genetics ; metabolism ; Calcium Channels, N-Type ; genetics ; metabolism ; Cell Line ; Enkephalin, Ala(2)-MePhe(4)-Gly(5)- ; pharmacology ; GTP-Binding Protein alpha Subunits, Gi-Go ; metabolism ; Genotype ; Humans ; Ion Channel Gating ; drug effects ; Kinetics ; Membrane Potentials ; Migraine with Aura ; genetics ; metabolism ; Mutation ; Phenotype ; Rats ; Receptors, Opioid, mu ; agonists ; metabolism ; Transfection

Author Keywords Familial hemiplegic migraine ; S218L mutation ; R192Q mutation ; Ca_v2.1 type calcium channel ; Ca_v2.1 subunit ; P/Q current ; G-protein ; G-protein coupled receptor ; μ -opioid receptor ; β -subunit.

Introduction

Familial hemiplegic migraine (FHM) is a rare, severe, monogenic subtype of migraine with aura, characterised by at least some degree of hemiparesis during the aura (1, 2). FHM-1 is caused by missense mutations in the gene CACNA1A encoding the Ca_v2.1 protein, the pore-forming subunit of Ca_v2.1 (formerly known as P/Q) calcium channels (14). To date, 19 different mutations have been described that are distributed over the four homologous domains of the Ca_v2.1 subunit. They generally affect structural determinants that are essential for channel activity including (i) the S4 transmembrane segments, thought to be voltage-sensor elements controlling channel activation, (ii) the S6 transmembrane segments, involved in the control of channel inactivation, and (iii) the P loops which form the ionic pore. Eleven of FHM-1 mutations have been characterized at the biophysical level (15), but only for one (the R192Q mutation that is associated with relatively mild, pure, FHM phenotype in patients (14)) the effects on G-protein regulation was reported (12). Ten out of 11 characterized mutations induce a hyperpolarizing shift of the voltage-dependence of channel activation, generally resulting in an increased channel opening probability already at mild potential values. However, additional effects have been observed on channel inactivation kinetics, current density, unitary conductance, open probability and selectivity (6, 8, 9, 13, 17, 18). A recently developed knock-in model expressing human pathogenic FHM-1 mutation R192Q revealed increased Ca²⁺ influx through mutant Ca_v2.1 channels and a decreased threshold and increased velocity of cortical spreading depression (CSD) (19, 20). CSD is the mechanism underlying migraine aura (10), and, in animal experiments, was shown to activate headache mechanisms (2). However, the exact molecular events leading to an increased susceptibility of CSD remain largely unresolved. A neuronal hyper-excitability due to a hyper-activity of Ca_v2.1 calcium channels seems most likely (15, 19, 20). The lower activation threshold of mutant Ca_v2.1 channels, associated with increased opening probability, may well trigger such hyper-activity. Alternatively, however, a reduction of inhibitory pathways may come in addition to produce a similar effect.

One important inhibitory regulation affecting Cav2.1 channels is produced by G-protein coupled receptor activation (for review see (3, 16)). This inhibition is based on the direct binding of the G $\beta\gamma$ signalling complex directly onto the Cav2.1 subunit (4). Recently, it was evidenced that this binding produces only the silencing of channel activity (“ON” effect), whereas G $\beta\gamma$ unbinding which follows channel activation induces an apparent set of biophysical modifications (“OFF” effects) that include: (i) a slowing of activation and inactivation kinetics, and (ii) a depolarizing shift of the voltage-dependence of channel activation (21). In that context, the kinetics of G $\beta\gamma$ dissociation from the channel is a critical factor in determining the probability that an inhibited channel recovers from G-protein inhibition during a burst of action potentials. Thereby, it should also influence the strength of persistence of a G-protein-related inhibitory pathway on synaptic signaling. Two factors were found to be essential in determining the speed of G $\beta\gamma$ dissociation: the voltage-dependence of channel activation and the kinetics of channel inactivation during membrane depolarization (21, 23). Indeed, activation at lower membrane potential values and faster inactivating channels were shown to be affected by the FHM-1 S218L mutation in the Cav2.1 subunit (18). This mutation is localized in the S4-S5 linker of the first domain and is associated with a particularly severe clinical phenotype of FHM and sometimes fatal delayed cerebral edema after minor head trauma in some mutation carriers (5, 7).

Therefore, we argued that, direct G-protein inhibition of mutated S218L Cav2.1 channels may be altered. Here we tested this hypothesis by transiently expressing, in HEK-293 cells, human Cav2.1 wild-type (Cav2.1^{WT}) or S218L mutant (Cav2.1^{S218L}) along with β_4 and $\alpha_2\delta-1_b$ auxiliary subunits, and the human μ -opioid receptor (hMOR). Direct G-protein regulation was induced by (D-Ala², N-Me-Phe⁴, glycinoI⁵)-Enkephalin (DAMGO) application. Application of DAMGO induces a maximal current inhibition that is similar for both wild-type and mutated Cav2.1 channels, suggesting that the FHM-1 S218L mutation does not alter the association of G $\beta\gamma$ onto the closed state of the channel. However, the recovery from G-protein inhibition following channel activation is considerably accelerated for Cav2.1^{S218L} channels, which is in accordance with the previously reported negative shift in the voltage-dependence of channel activation and the faster channel inactivation. In light of these data, G-protein regulation of the R192Q mutant (Cav2.1^{R192Q}, that is associated with a less severe clinical phenotype) was also investigated with similar protocols, and comparable alteration of G-protein regulation were observed, albeit less pronounced. Taken together, these observations indicate that the FHM-1 S218L and R192Q mutations promote Cav2.1 current recovery from direct G-protein inhibition in line with their respective degree of clinical phenotype, and thus decrease the inhibitory influence of this signalling pathway. These effects on G-protein regulation should contribute, along with the main biophysical effects on channel activation, to render the neuronal network hyperexcitable, possibly as a consequence of reduced presynaptic inhibition, and help explain the pathophysiology of FHM.

Materials and Methods

Material

The cDNAs used in this study were human Cav2.1 (GenBank accession number AF004883), rat β_4 (L02315), rat $\alpha_2\delta-1_b$ (NM012919) and human μ -opioid receptor (hMOR, obtained from the UMR cDNA Resource Center www.cdna.org) (AY521028). The cDNA encoding for the Cav2.1^{S218L} mutant protein is described in (18). The cDNA encoding for the Cav2.1^{R192Q} mutant was kindly provided by Dr. J. Striessnig, University of Innsbruck, Austria. (D-Ala², N-Me-Phe⁴, glycinoI⁵)-Enkephalin (DAMGO) was purchased from Bachem (Budendorf, Germany).

Transient expression in HEK-293

Human embryonic kidney 293 (HEK-293) cells were grown in a Dulbecco's modified Eagle's culture medium containing 10% foetal bovine serum and 1% penicillin/streptomycin (all products were purchased from Invitrogen) and maintained under standard conditions at 37°C in a humidified atmosphere containing 5% CO₂. Cells were transfected using the jetPEITM transfection reagent (Qbiogene, OH, USA) according to the protocol provided in the kit with cDNAs encoding Cav2.1^{WT} or Cav2.1^{S218L} mutant subunit along with β_4 , $\alpha_2\delta-1_b$, hMOR and the enhanced green fluorescent protein plasmid (pEGFP; Clontech, CA, USA). Two days following transfection, cells were briefly split at 10% confluence using PBS without calcium and magnesium and patch-clamp recording was performed 4 hours later from fluorescent cells.

Patch-clamp recordings

Ba²⁺ currents were recorded in the whole-cell configuration of the patch-clamp technique at room temperature (22–24°C) in a bathing medium containing (in millimolar): BaCl₂ 5, KCl 5, MgCl₂ 1, NaCl 128, TEA-Cl 10, D-glucose 10, HEPES 10 (pH 7.4 with NaOH). Patch pipettes were filled with a solution containing (in millimolar): CsCl 110, Mg-ATP 3, Na-GTP 0.5, MgCl₂ 2.5, D-glucose 5, EGTA 10, HEPES 10 (pH 7.4 with CsOH), and had a resistance of 2–4 M Ω . Whole-cell patch-clamp recording were performed using an Axopatch 200B amplifier (Axon Instruments, Union City, CA). Acquisition and analyses were performed using pClamp 6 and Clampfit 9 software, respectively (Axon Instruments). All traces were corrected on-line for leak and capacitance currents, digitized at 10 KHz and filtered at 2 KHz. DAMGO was applied at 10 μ M by superfusion of the cells at 4 mL/min and all recordings were performed within 1 min after DAMGO produced maximal current inhibition in order to minimized voltage-independent G-protein regulation and hMOR desensitization.

Analyses of the parameters of G-protein regulation

The method used to extract all biophysical parameters of G-protein regulation (GI_{t_0} , the initial extent of G-protein inhibition before the start of depolarisation, τ , the time constant of G-protein unbinding from the channel, and RI, the extent of recovery from inhibition at the end of a 200 ms test pulse) was described in (22). Briefly, subtracting I_{DAMGO} from $I_{Control}$ results in I_{Lost} , the evolution of the lost current under G-protein activation. $I_{Control}$ and I_{Lost} are then extrapolated to $t = 0$ ms (the start of the depolarisation) by fitting traces with an exponential function in order to determine GI_{t_0} , the maximal extent of G-protein inhibition. I_{DAMGO} without unbinding ($I_{DAMGO\ wo\ unbinding}$) represents an estimate of the amount of control current that is present in I_{DAMGO} and is obtained by the following equation: $I_{DAMGO\ without\ unbinding} = I_{Control} \times (1 - (I_{Lost_{t_0}}/I_{Control_{t_0}}))$. Subtracting $I_{DAMGO\ wo\ unbinding}$ from I_{DAMGO} results in $I_{G-protein\ unbinding\ with\ inactivation}$, the evolution of inhibited current that recovers from G-protein inhibition following depolarisation. $I_{G-protein\ unbinding\ with\ inactivation}$ is divided by the fit trace (normalized to 1) describing inactivation kinetics of the control current in order to reveal the net kinetics of G-protein dissociation ($I_{G-protein\ unbinding}$) from the channels. A fit of $I_{G-protein\ unbinding}$ by a mono-exponential decrease provides the time constant τ of G-protein dissociation from the channel. The percentage of recovery from G-protein inhibition (RI) after 200 ms test pulse is measured as $RI = (I_{DAMGO} - I_{DAMGO\ wo\ unbinding})/(I_{Control} - I_{DAMGO\ wo\ unbinding}) \times 100$.

Mathematical and statistical analyses

Current-voltage relationships (I/V) were fitted with the modified Boltzmann equation $I(V) = (G_{max} \times (V - E))/(1 + \exp(-(V - V_{1/2})/k))$ where $I(V)$ represents the maximal current amplitude in response to a depolarization at the potential V , G_{max} is the maximal conductance, E is the inversion potential of Ba^{2+} , and k is a slope factor. All data are given as mean \pm S.E.M for n number observations and statistical significance (p) was calculated using Student's t test.

Results

The FHM-1 S218L mutation alters the biophysical properties of $Ca_v2.1/\alpha_2\delta-1_b/\beta_4$ channels expressed in HEK-293 cells

To characterize the biophysical impact of the FHM-1 S218L mutation, human $Ca_v2.1^{WT}$ or $Ca_v2.1^{S218L}$ mutant channels were transiently expressed in HEK-293 cells along with neuronal β_4 (the predominant β -subunit associated with $Ca_v2.1$ channels in the brain) and $\alpha_2\delta-1_b$ auxiliary subunits. Whole-cell barium (Ba^{2+}) currents were recorded two days after transfection from cells expressing the two various channel subunit combinations. Average current traces are shown in Fig. 1a in response to a 500 ms membrane depolarisation ranging between -40 and 40 mV from a holding potential of -90 mV. The voltage-dependencies of activation of wild-type and mutant $Ca_v2.1$ channels were determined (Fig. 1b). The mean half-activation potential of the mutant $Ca_v2.1$ channel is significantly shifted ($p < 0.001$) towards more negative voltages by 4.8 mV on average from -8.2 ± 0.4 mV ($n = 13$, wild-type) to -13.0 ± 0.6 mV ($n = 13$, mutant). No significant differences in current densities were observed between both channel types (Fig. 1b). However, there is a slight tendency to observe larger current densities for the mutant channel at potential values inferior at 0 mV. Given the shift to the left of the voltage-dependence of activation of the mutant channel, these results suggest that the mutant channel expressed as well as the wild-type one (Fig. 1b). In contrast, significant differences were observed in activation and inactivation kinetics. The activation kinetics of the currents carried by S218L mutant channels were significantly accelerated ($p < 0.001$) at all voltages studied as evidenced by the 3.2- (10 mV) to 4.2-fold (30 mV) shorter time to peak compared to wild-type channels (Fig. 1c). Channel inactivation kinetics is best fitted by a mono-exponential decay in the case of the wild-type channel, whereas two exponential components are required to fit the mutant channel inactivation kinetics (Fig. 1d, dashed line). The slow component of the inactivation kinetics of the mutant channel is significantly faster by 2.6- (0 mV, $p < 0.001$) to 1.4-fold (20 mV, $p = 0.003$) than the inactivating component of the wild-type channel for membrane potential values equal or under 20 mV; no significant difference is observed above 20 mV. The fast inactivating component of the mutant channel is between 5.1- (-10 mV, $p < 0.001$) and 24.2-fold (40 mV, $p < 0.001$) significantly faster than its slow component. The contribution of each component to the extent of inactivation is shown in Fig. 1e. The fast component of the mutant channel represents a minor fraction of the inactivating current that decreases from $18.9 \pm 2.0\%$ (-10 mV) to $6.8 \pm 0.1\%$ (40 mV). The total amount of current inactivation rises from $50.2 \pm 7.5\%$ (-10 mV) to $74.3 \pm 4.0\%$ (40 mV) for the wild-type channel compared to $63.6 \pm 5.9\%$ (-10 mV) to $89.7 \pm 2.6\%$ (40 mV) for the mutant channel, a difference that is not significant except at -10 and 40 mV probably due to the difficulty to precisely measure this parameter at these two extreme membrane potentials. Analysis of integrated whole cell currents reveals that the S218L mutation differentially affects calcium entry depending of membrane potentials (Fig. 1f). While the mutation leads to an increase in calcium entry during the time course of the current for potential values below -10 mV, at -10 mV it promotes calcium influx only during the initial phase of current activation and has an opposite effect for potential values under -10 mV due to the faster inactivation of the mutant. Taken together, these results indicate that the FHM-1 S218L mutation produces three major biophysical modifications of $Ca_v2.1/\beta_4/\alpha_2\delta-1_b$ channels at the whole-cell level: a hyperpolarizing shift of the voltage-dependence of channel activation, and faster channel activation and inactivation. These findings confirm earlier observations in experiments that expressed $Ca_v2.1^{WT}$ or $Ca_v2.1^{S218L}$ channels together with

other auxiliary β - (β_{2e} or β_{1b}) and $\alpha_2\delta$ -1_b subunits (18). Since we have previously shown that these parameters critically affect the direct G-protein inhibition of voltage-gated calcium channels (21, 23), this study was pursued to investigate how the FHM-1 S218L mutation could affect the inhibition of Cav2.1 channels.

The FHM-1 S218L mutation does not affect maximal current inhibition by G-proteins

It is essential to measure the extent of G-protein inhibition at the start of the depolarisation to avoid the important, but confounding, fraction of recovery from inhibition that has already occurred when current amplitudes are measured at their peak. Representative current traces for wild-type and mutant channels are shown at 0 and 20 mV in the top panels of Fig. 2a and 2b both before ($I_{Control}$) and during DAMGO application (I_{DAMGO}). According to our recently developed method of analysis of G-protein regulation (22, 23), the Lost current traces were extracted (I_{Lost}) by subtracting I_{DAMGO} from $I_{Control}$. I_{Lost} provides the time course of the lost current following G-protein activation, affected by both the recovery from G-protein inhibition following channel activation and by the inactivation process. Hence, current inhibition measured from the levels of I_{Lost} and $I_{Control}$ when extrapolated at $t = 0$ ms provides the net maximal G-protein inhibition (GI_0) before these processes (current recovery and channel inactivation) have taken place (Fig. 2a, b, lower panels). Average GI_0 values were reported as a function of membrane potential (Fig. 2c). As expected for an inhibition at $t = 0$ ms, the maximal current inhibition by G-proteins is not voltage-dependent. This inhibition varies between $55.8 \pm 3.8\%$ (-10 mV) and $51.2 \pm 5.3\%$ (30 mV) for the wild-type channel and is not significantly different for the mutant channel (between $53.1 \pm 2.3\%$ (0 mV) and $49.9 \pm 3.3\%$ (20 mV)). More importantly, also no significant differences were observed in the maximal current inhibition achieved by DAMGO application between wild-type and mutant channels at all membrane potentials studied. This suggests that the FHM-1 S218L mutation does not affect binding of $G_{\beta\gamma}$ onto the closed state of Cav2.1 channels ("ON" effect).

Next we searched for possible "OFF" effects of G-protein regulation for Cav2.1^{S218L} channels. One characteristic "OFF" effect is the apparent slowing of current activation kinetics under DAMGO inhibition, which results from a channel opening- and time-dependent recovery from inhibition (21). The current traces shown in Fig. 2a, b (top panels) illustrate that DAMGO application produces an important slowing of activation kinetics for wild-type channels, whereas the extent of this effect appears greatly diminished for the FHM-1 S218L mutation. This was further quantified in Fig. 2d where the shift of the time to peak of the current follows an exponential decay from 76.8 ± 7.4 ms (-10 mV, $n = 13$) to 12.2 ± 1.5 ms (40 mV, $n = 13$) for the wild-type channel. Far less voltage-dependence is seen for the S218L mutant since the shift of current time to peak varies only between 10.0 ± 2.5 ms (10 mV, $n = 13$) and 6.9 ± 2.0 ms (30 mV, $n = 13$). The differences between the two channels remain statistical significant at all voltages ($p < 0.01$ or less) except at 30 and 40 mV where convergence between mean values is observed. These data strongly suggest a difference in the kinetics of recovery from G-protein inhibition.

The FHM-1 S218L mutation induces faster G-protein dissociation upon channel activation

The two parameters that characterize the "OFF" components of G-protein regulation of Cav2.1 voltage-gated calcium channels, i.e. the time constant of current recovery (τ) and the maximal extent of current recovery from inhibition (RI), were extracted from the data using our recently published method (22, 23). Representative current traces before and under DAMGO application are shown for wild-type and S218L mutant Cav2.1 channels at 0 and 20 mV step depolarisation from a holding potential of -90 mV (Fig. 3a, b, top panels). Corresponding current traces that describe the evolution of current recovery ($I_{G-protein\ unbinding}$) were best fitted with a mono-exponential decrease providing τ values (Fig. 3a, b, middle panels, red dashed line). The RI values were extracted at 200 ms depolarization by comparing the level of current recovery from DAMGO traces (I_{DAMGO}) to non-inhibited control currents ($I_{Control}$) and the fraction of control currents under G-protein regulation ($I_{DAMGO\ wo\ unbinding}$). According to the τ values reported below, measuring RI values at 200 ms ensures that the recovery process from G-protein inhibition is completed. Significantly faster time constants (i.e. average τ values, $p = 0.028$ or less) were observed for the Cav2.1^{S218L} channel at all voltages compared to the Cav2.1^{WT} channel (Fig. 3c): time constants decreased from 41.0 ± 5.4 ms (-10 mV, $n = 13$) to 6.6 ± 0.6 ms (30 mV, $n = 13$) for the wild-type channel, whereas a 1.7- to 2.3-fold faster τ values were observed for the mutant which ranged from 23.4 ± 4.0 ms (-10 mV, $n=13$) to 2.9 ± 0.5 ms (30 mV, $n = 13$). Also, significantly smaller RI values ($p < 0.01$ or less) were observed for the mutant channel at all membrane potentials except at -10 mV (Fig. 3d). Wild-type RI values ranged from $45.8 \pm 5.5\%$ (-10 mV, $n = 13$) to $64.2 \pm 4.3\%$ (20 mV, $n = 13$), whereas RI values for the S218L mutant show a diminished voltage-dependence and ranged from $30.6 \pm 2.7\%$ (20 mV, $n = 13$) to $35.6 \pm 5.1\%$ (30 mV, $n = 13$). The faster current recovery observed for the Cav2.1^{S218L} channel, associated to a smaller extent of recovery, is consistent with previously published results, in which voltage-dependent channel inactivation not only promotes recovery from G-protein inhibition but also reduces the temporal window of the recovery process (23). Combined, these two parameters explain the reduced shift of the time to peak of the current of the S218L mutant channel under G-protein regulation.

The FHM-1 R192Q mutation behaves similarly to the S218L mutation with regard to G-protein regulation

In order to extend the observations made with the S218L mutation, another FHM-1 mutation, R192Q, was also investigated in the same experimental conditions. Fig. 4 summarizes the main biophysical properties of Cav2.1^{R192Q}/ $\beta_4/\alpha_2\delta$ -1_b channels. Representative

average current traces ($n = 11$) of $\text{Ca}_v2.1^{\text{R192Q}}$ mutant channels expressed along with β_4 and $\alpha_2\delta-1_b$ are shown in Fig. 4a. Average I-V relationships are shown in Fig. 4b and confirm earlier findings (6) that the mutation induces an increase in current density (average stimulation of 1.9-fold at 0 mV). As for the S218L mutation, an average hyperpolarizing shift of channel activation is observed although of lesser amplitude (half-activation potential of -10.7 ± 0.9 mV ($n = 11$) compared to -8.2 ± 0.4 mV ($n = 13$) for wild-type). A slight decrease in time to peak of the current is observed although this effect remains non significant (Fig. 4c). With regard to inactivation kinetics, currents follow a single exponential decrease similarly to wild-type currents, with faster inactivation kinetics at potential values below 10 mV (1.8-fold decrease at 0 mV) (Fig. 4d). Also, the inactivating component is accentuated at lower voltages for the R192Q mutation (for instance 15% more of inactivation at 0 mV) (Fig. 4e). Average integrals of current densities are shown at -20 mV, -10 mV, 0 mV and 20 mV for $\text{Ca}_v2.1^{\text{R192Q}}$ channels in Fig. 4f and indicate that contrary to the S218L mutation, the R192Q mutation promotes calcium influx at all membrane potential values tested. Taken together, these results indicate that this mutation shares similarities with the S218L mutation regarding the voltage-dependence of activation, and activation and inactivation kinetics, although all effects are less pronounced. One major difference concerns the current density which was previously interpreted as being due to an increase in the opening probability of the $\text{Ca}_v2.1^{\text{R192Q}}$ mutated channel (6). Nevertheless, all the biophysical changes are susceptible to alter G-protein regulation in a similar manner than that observed for S218L.

This regulation was investigated as shown in Fig. 5. Representative traces allowing the measurements of maximal G-protein inhibition (GI_{10}) are shown in Fig. 5a at 0 mV (left panel) and 20 mV (right panel). As for the S218L mutation, maximal G-protein inhibition ("ON" effect) of $\text{Ca}_v2.1^{\text{R192Q}}$ channels is similar to that of the wild-type channel (Fig. 5b). In contrast, a significant reduction was observed in the shift of the current time to peak induced by DAMGO application on $\text{Ca}_v2.1^{\text{R192Q}}$ channels (Fig. 5c) suggesting an alteration of G-protein dissociation from the channel. For instance, a 2.2-fold reduction was observed at 0 mV in the shift of the current time to peak. The parameters of G-protein dissociation (time constant of dissociation, τ , and the extent of recovery from inhibition, RI) were extracted as shown in Fig. 5d. Average τ values obtained for $\text{Ca}_v2.1^{\text{R192Q}}$ channels are shown in Fig. 5e as a function of membrane potentials. As for the S218L mutation, the dissociation of G-proteins from $\text{Ca}_v2.1^{\text{R192Q}}$ mutated channel is accelerated particularly for potentials below 10 mV (1.4-fold at 0 mV, compared to wild-type). In contrast to the S218L mutation however, the R192Q mutation does not affect the maximal extent of recovery from G-protein inhibition. This observation is consistent with the mild effect of this mutation on channel inactivation.

Discussion

This study shows that the FHM-1 S218L mutation of the human $\text{Ca}_v2.1$ subunit when expressed in HEK-293 cells along with β_4 and $\alpha_2\delta-1_b$ auxiliary subunits, affects both intrinsic biophysical properties of $\text{Ca}_v2.1$ channels and direct G-protein regulation of the channel. Similar observations are made for the FHM-1 R192Q mutation, although changes are less pronounced, which seems in line with the less severe clinical phenotype of that mutation (7, 14).

Biophysical consequences of the FHM-1 S218L mutation on $\text{Ca}_v2.1$ channel activity

It was previously shown that the S218L mutation, introduced in the human $\text{Ca}_v2.1$ subunit and expressed in HEK-293 cells or in cerebellar granule cells along with the β_{2e} or β_{1b} and $\alpha_2\delta-1_b$ auxiliary subunits, (i) promotes channel activation at lower membrane potential and (ii) induces faster inactivation kinetics during relatively short depolarisation (< 200 – 300 ms) and introduces a component of current that inactivates very slowly and results in a lower extent of inactivation during long depolarisation (> 500 ms) (18). Here, the human $\text{Ca}_v2.1^{\text{WT}}$ or $\text{Ca}_v2.1^{\text{S218L}}$ channels were expressed in HEK-293 cells along with the preferentially neuronal associated β_4 and $\alpha_2\delta-1_b$ auxiliary subunits (11). Under these experimental conditions, the FHM-1 S218L mutation also induces a hyperpolarized shift of the voltage-dependence of $\text{Ca}_v2.1$ channel activation as well as faster inactivation kinetics at the whole-cell level. However, contrary to earlier studies, no statistical difference between wild-type and mutant channels was observed in the extent of inactivation, as extrapolated beyond the 500 ms depolarisation pulse. In addition, the FHM-1 S218L mutation is found here to induce faster activation kinetics. Whether this effect is specific of the presence of the β_4 subunit or not remains to be seen. It was not reported in the presence of the β_{2e} or β_{1b} subunits (18), but a visual examination of the current traces from this earlier report seem to show that it is the case. These results indicate that although the FHM-1 S218L mutation produces some common biophysical alterations regardless of the type of β subunit used, some modifications might be β subunit-dependent.

The FHM-1 S218L mutation differentially affects "ON" and "OFF" G-protein regulation of $\text{Ca}_v2.1$ channels

One of the major inhibitory pathway controlling voltage-gated calcium channels at the synaptic level is mediated by G-protein coupled receptor activation. This inhibition is recognized by a strong ionic current inhibition ("ON" effect), whereas the process of channel activation produces deinhibition, which is characterized by slowed current kinetics and a more or less pronounced extent of current recovery ("OFF" effects). Hence, if current inhibition finally only represents an index of the total amount of channels potentially affected by direct G-protein inhibition, current deinhibition really reflects the importance of this regulation under channel activity. In this study "ON" and "OFF" G-protein regulation parameters were quantified using our recently developed method (22, 23). Hence, G-protein

inhibition, measured at the start of the depolarisation, before the initiation of the process of recovery, is not affected by the FHM-1 S218L mutation. This suggests that the S218L mutation does not affect the binding of $G_{\beta\gamma}$ onto the closed-state of the channel, which is consistent with the fact that this mutation is localized in the IS4-S5 linker of the $Ca_v2.1$ subunit. It is not expected to affect one of the structural channel determinants known to be involved in $G_{\beta\gamma}$ binding (i.e. the I-II loop, the amino-terminus or the carboxy-terminal region of the $Ca_v2.1$ subunit). We did observe that the S218L mutation critically affects the "OFF" effects of $Ca_v2.1$ calcium channel regulation by G-proteins as the time constant of current recovery from inhibition (τ) was drastically accelerated by 1.7- to 2.3-fold for $Ca_v2.1^{S218L}$ channels depending on membrane potential values. In contrast, the maximal extent of current recovery, measured 200 ms after the start of the depolarisation, at a time point where the process of recovery is maximal according to time constant values, is clearly diminished by the mutation. These results are consistent with previous data showing that the molecular process of channel inactivation accelerates the recovery from inhibition, but reduces the temporal window in which the process can take place, thereby reducing the maximal extent of current recovery (23). We cannot exclude that the lower activation threshold of the mutant channel could also contribute to accelerate the recovery from G-protein inhibition, since we have previously shown that the time constant of G-protein dissociation follows the voltage-dependence of channel opening (21). Nevertheless, we can reasonably argue that, in a physiological context, i.e. during burst of action potentials, the main parameter that controls channel activity under G-protein inhibition is the kinetics of the recovery process. Hence, by promoting $Ca_v2.1$ channels deinhibition from G-proteins, the FHM-1 S218L mutation diminishes the strength of this negative feedback, and is therefore likely to contribute to the hyperactivity of $Ca_v2.1$ channels and to the neuronal hyperexcitability, that is an emerging theme in the pathophysiology of FHM.

The FHM-1 R192 mutation also affects direct G-protein regulation of $Ca_v2.1$ channels

Similarly to that we observed with the S218L mutation, the R192Q mutation does not affect the maximal G-protein inhibition of $Ca_v2.1$ channels (i.e., also suggesting that it does not affect G-proteins association to the channel), but promotes current recovery from G-protein inhibition. This conclusion contrasts with that of a similar study on the R192Q mutation, for which a reduced G-protein inhibition was reported (12). However, in that study, G-protein inhibition levels were measured at the peak of the currents, at time points where significant recovery from G-protein inhibition may already have occurred for the mutant channel if this mutation also accelerates G-protein dissociation, thereby artificially providing the impression that the "ON" effect is diminished.

Potential implication in the pathogenesis of the FHM-1

Cortical spreading depression (CSD) is commonly believed to underlie the migraine aura, and probably headache mechanisms (2, 10, 19). However, what occurs at the very first stages of CSD is largely unclear. Neuronal silencing in CSD follows a short period of intense neuronal firing. It is conceivable that $Ca_v2.1$ calcium channels could be the actors initiating the process. The diminution of the channel activation threshold induced by the FHM-1 S218L mutation (and R192Q mutation) represents a potential intrinsic factor, which may easily contribute to neuronal hyperexcitability in patients. Moreover, the hyperactivity of $Ca_v2.1$ channels could also be triggered by a diminution of the inhibitory pathway carried by G-proteins. Thus, the FHM-1 S218L mutation contributes to maintain calcium influx through $Ca_v2.1$ channels especially during high synaptic activity by promoting channel deinhibition. Hence, the combined diminution of channel activation threshold and decrease of the inhibitory pathway may represent the initiating molecular events of CSD, ultimately leading to migraine.

Acknowledgements:

We warmly thank Dr. Daniela Pietrobon for helpful comments and discussion on the manuscript. We are very grateful to Dr. J. Striessnig (University of Innsbruck, Austria) for the gift of the $Ca_v2.1^{R192Q}$ cDNA. We acknowledge financial support of Inserm. Additional support was obtained from EU project EUROHEAD (LSHM-CT-2004-504837).

Abbreviations: The following abbreviations have been used

DAMGO: (D-Ala², N-Me-Phe⁴, glycinol⁵)-Enkephalin

FHM-1: familial hemiplegic migraine type 1

hMOR: human μ -opioid receptor

GI: G-protein inhibition

RI: recovery from inhibition

CSD: cortical spreading depression

NS: non statistically significant

References:

1. 2004; The International Classification of Headache Disorders: 2nd edition. Cephalalgia. 24: (Suppl 1) 9- 160
2. Bolay H , Reuter U , Dunn AK , Huang Z , Boas DA , Moskowitz MA 2002; Intrinsic brain activity triggers trigeminal meningeal afferents in a migraine model. Nat Med. 8: 136- 142
3. De Waard M , Hering J , Weiss N , Feltz A 2005; How do G proteins directly control neuronal Ca^{2+} channel function?. Trends Pharmacol Sci. 26: 427- 436

- 4. De Waard M , Liu H , Walker D , Scott VE , Gurnett CA , Campbell KP 1997; Direct binding of G-protein $\beta\gamma$ complex to voltage-dependent calcium channels. *Nature*. 385 : 446- 450
- 5. Fitzsimons RB , Wolfenden WH 1985; Migraine coma. Meningitic migraine with cerebral oedema associated with a new form of autosomal dominant cerebellar ataxia. *Brain*. 108 : (Pt 3) 555- 577
- 6. Hans M , Luvisetto S , Williams ME , Spagnolo M , Urrutia A , Tottene A , Brust PF , Johnson EC , Harpold MM , Stauderman KA , Pietrobon D 1999; Functional consequences of mutations in the human α_{1A} calcium channel subunit linked to familial hemiplegic migraine. *J Neurosci*. 19: 1610- 1619
- 7. Kors EE , Terwindt GM , Vermeulen FL , Fitzsimons RB , Jardine PE , Heywood P , Love S , van den Maagdenberg AM , Haan J , Frants RR , Ferrari MD 2001; Delayed cerebral edema and fatal coma after minor head trauma: role of the CACNA1A calcium channel subunit gene and relationship with familial hemiplegic migraine. *Ann Neurol*. 49: 753- 760
- 8. Kraus RL , Sinnegger MJ , Glossmann H , Hering S , Striessnig J 1998; Familial hemiplegic migraine mutations change α_{1A} Ca^{2+} channel kinetics. *J Biol Chem*. 273: 5586 - 5590
- 9. Kraus RL , Sinnegger MJ , Koschak A , Glossmann H , Stenirri S , Carrera P , Striessnig J 2000; Three new familial hemiplegic migraine mutants affect P/Q-type Ca^{2+} channel kinetics. *J Biol Chem*. 275: 9239- 9243
- 10. Lauritzen M 1994; Pathophysiology of the migraine aura. The spreading depression theory. *Brain*. 117 : (Pt 1) 199- 210
- 11. Ludwig A , Flockerzi V , Hofmann F 1997; Regional expression and cellular localization of the α_1 and β subunit of high voltage-activated calcium channels in rat brain. *J Neurosci*. 17: 1339- 1349
- 12. Melliti K , Grabner M , Seabrook GR 2003; The familial hemiplegic migraine mutation R192Q reduces G-protein-mediated inhibition of P/Q-type ($Ca_v2.1$) calcium channels expressed in human embryonic kidney cells. *J Physiol*. 546: 337- 347
- 13. Mullner C , Broos LA , van den Maagdenberg AM , Striessnig J 2004; Familial hemiplegic migraine type 1 mutations K1336E, W1684R, and V1696I alter $Ca_v2.1$ Ca^{2+} channel gating: evidence for β -subunit isoform-specific effects. *J Biol Chem*. 279: 51844- 51850
- 14. Ophoff RA , Terwindt GM , Vergouwe MN , van Eijk R , Oefner PJ , Hoffman SM , Lamerdin JE , Mohrenweiser HW , Bulman DE , Ferrari M , Haan J , Lindhout D , van Ommen GJ , Hofker MH , Ferrari MD , Frants RR 1996; Familial hemiplegic migraine and episodic ataxia type-2 are caused by mutations in the Ca^{2+} channel gene CACNL1A4. *Cell*. 87: 543- 552
- 15. Pietrobon D 2005; Migraine: new molecular mechanisms. *Neuroscientist*. 11: 373- 386
- 16. Tedford HW , Zamponi GW 2006; Direct G protein modulation of Ca_v2 calcium channels. *Pharmacol Rev*. 58: 837- 862
- 17. Tottene A , Fellin T , Pagnutti S , Luvisetto S , Striessnig J , Fletcher C , Pietrobon D 2002; Familial hemiplegic migraine mutations increase Ca^{2+} influx through single human $Ca_v2.1$ channels and decrease maximal $Ca_v2.1$ current density in neurons. *Proc Natl Acad Sci U S A*. 99: 13284- 13289
- 18. Tottene A , Pivotto F , Fellin T , Cesetti T , van den Maagdenberg AM , Pietrobon D 2005; Specific kinetic alterations of human $Ca_v2.1$ calcium channels produced by mutation S218L causing familial hemiplegic migraine and delayed cerebral edema and coma after minor head trauma. *J Biol Chem*. 280: 17678- 17686
- 19. van de Ven RC , Kaja S , Plomp JJ , Frants RR , van den Maagdenberg AM , Ferrari MD 2007; Genetic models of migraine. *Archives of neurology*. 64: 643- 646
- 20. van den Maagdenberg AM , Pietrobon D , Pizzorusso T , Kaja S , Broos LA , Cesetti T , van de Ven RC , Tottene A , van der Kaa J , Plomp JJ , Frants RR , Ferrari MD 2004; A CACNA1A knockin migraine mouse model with increased susceptibility to cortical spreading depression. *Neuron*. 41: 701- 710
- 21. Weiss N , Arnoult C , Feltz A , De Waard M 2006; Contribution of the kinetics of G protein dissociation to the characteristic modifications of N-type calcium channel activity. *Neurosci Res*. 56: 332- 343
- 22. Weiss N , De Waard M 2007; Introducing an alternative biophysical method to analyze direct G protein regulation of voltage-dependent calcium channels. *J Neurosci Methods*. 160: 26- 36
- 23. Weiss N , Tadmouri A , Mikati M , Ronjat M , De Waard M 2007; Importance of voltage-dependent inactivation in N-type calcium channel regulation by G-proteins. *Pflugers Arch*. 454: 115- 129

Fig. 1

The familial hemiplegic migraine type 1 (FHM-1) mutation S218L induces kinetic and voltage alterations of Cav_v2.1 calcium channel activity. **a** Average set of whole cell current traces for Cav_v2.1^{WT}/β₄/α₂δ-1_b (n = 13) and Cav_v2.1^{S218L}/β₄/α₂δ-1_b (n = 13) channels obtained by 500 ms depolarization values ranging between -40 and 40 mV. Holding potential is -90 mV. **b** Average current-voltage relationships for currents measured at their peak values. Inset: average half-activation potentials for wild-type (filled circles) and mutant (open circles) channels. **c** Representative current traces at 0 mV showing differences in activation kinetics (top panel). Symbols illustrate the time to peak. Average current time to peak values as a function of test potentials for wild-type (filled circles, n = 13) and mutant (open circles, n = 13) channels (lower panel). **d** Representative current traces at 0 mV for wild-type and mutant channels showing differences in inactivation kinetics (top panel). Inactivating currents were fitted (dashed line) by a mono-exponential equation (wild-type channels, filled circle) or a bi-exponential equation (mutant channels, open square for fast component and open circle symbol for slow component). Average inactivation time constants for both conditions (n = 13 for control and n = 13 for mutation) as a function of test potential (lower panel). The y-axis presents a break point for display purposes. **e** Average proportion of each inactivating component for wild-type (filled bars, n = 13) and mutants channels (open bars, n = 13). **f** Average integrated whole cell currents for wild-type (filled circle, n = 13) and S218L mutant (open circle, n = 13) channels at -20 mV, -10 mV, 0 mV and 20 mV. Vertical scale: 500, 1000, 2000 and 1000 pA. ms. pF⁻¹ respectively. Data are presented as mean ± S.E.M for n studied cells. Statistical t test: NS, non significant; *, p ≤ 0.05; ***, p ≤ 0.001.

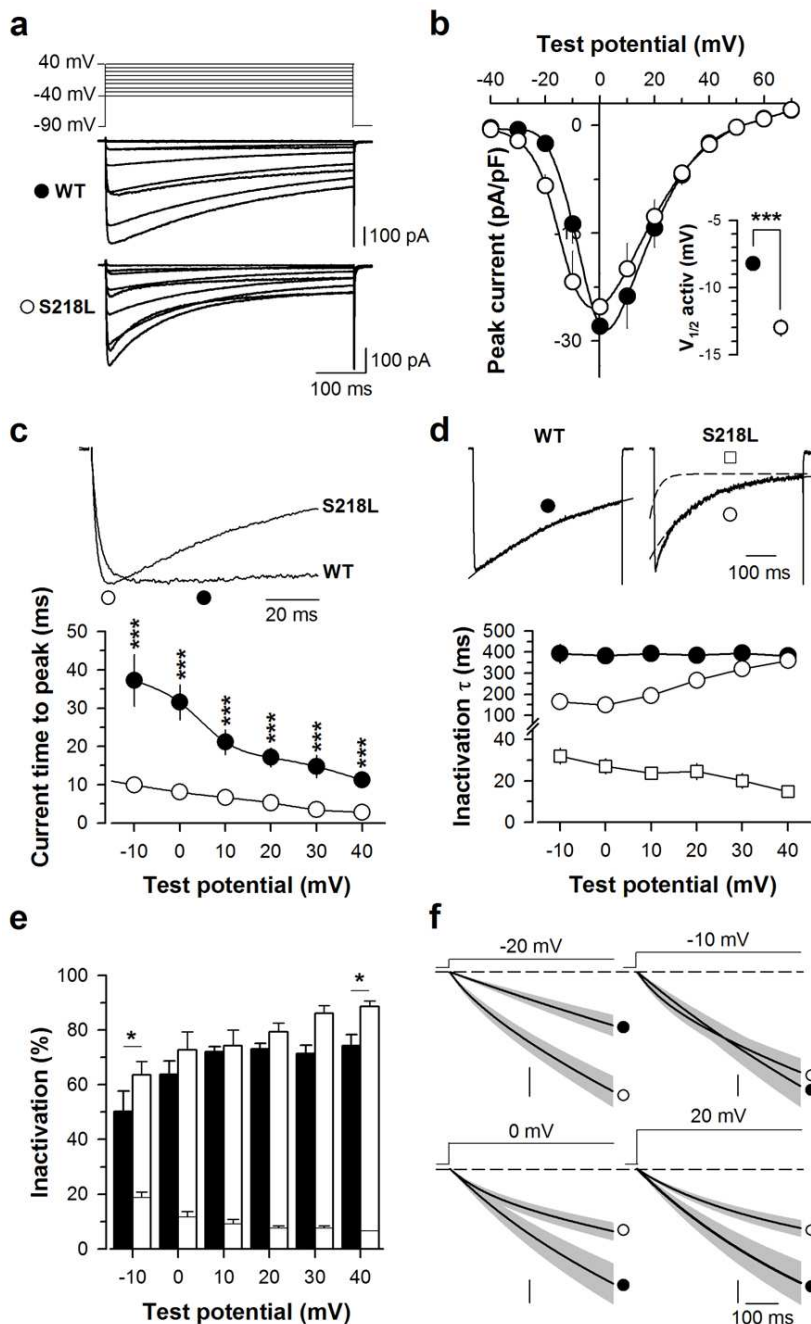


Fig. 2

The S218L mutation does not affect the maximal G-protein inhibition of $\text{Ca}_v2.1$ currents. **a** Representative normalized current traces elicited at 0 and 20 mV before (I_{Control}) and under 10 μM DAMGO application (I_{DAMGO}) for $\text{Ca}_v2.1^{\text{WT}}$ channels with β_4 and $\alpha_2\delta-1_b$ auxiliary subunits (top panel). Corresponding traces allowing the measurement of the maximal DAMGO inhibition at the start of the depolarisation (GI_{t_0}) (bottom panel). I_{Control} and I_{Lost} (obtained by subtracting I_{DAMGO} from I_{Control}) were fitted (red dashed line) by a mono- and a double-exponential, respectively, in order to better estimate GI_{t_0} . The arrow indicates the start of the depolarisation. Scale: 50 ms. **b** Legend as in (a) but for cells expressing $\text{Ca}_v2.1^{\text{S218L}}$ channels with β_4 and $\alpha_2\delta-1_b$ auxiliary subunits. **c** Bar chart representation of GI_{t_0} for $\text{Ca}_v2.1^{\text{WT}}$ (filled bars, $n = 13$) and $\text{Ca}_v2.1^{\text{S218L}}$ (open bars, $n = 13$) channels as a function of membrane potential. **d** Shift of the current time to peak induced by DAMGO application for $\text{Ca}_v2.1^{\text{WT}}/\beta_4/\alpha_2\delta-1_b$ channels (filled circle, $n = 13$) and $\text{Ca}_v2.1^{\text{S218L}}/\beta_4/\alpha_2\delta-1_b$ channels (open circle, $n = 13$) as a function of membrane potential. Data are presented as mean \pm S.E.M for n studied cells. Statistical t test: NS, non-significant; **, $p \leq 0.01$; ***, $p \leq 0.001$.

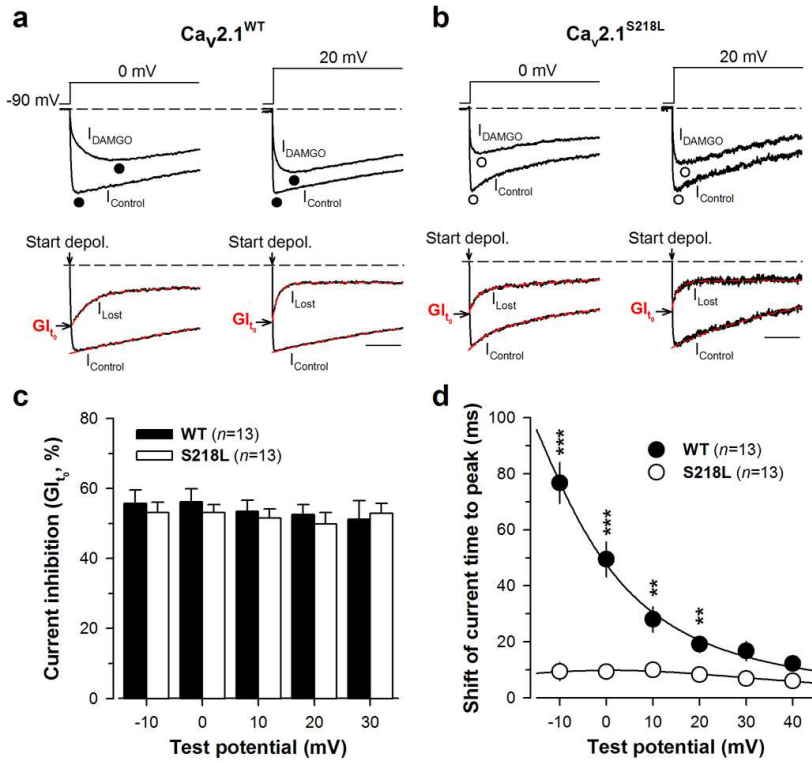


Fig. 3

The FHM-1 S218L mutation promotes current recovery from G-protein inhibition. **a** Representative normalized current traces for $Ca_v2.1^{WT}/\beta_4/\alpha_2\delta-1_b$ channels elicited at 0 and 20 mV before ($I_{Control}$) and during DAMGO application (I_{DAMGO}) (top panel). Corresponding normalized $I_{G\text{-protein unbinding}}$ traces fitted by a mono-exponential decrease (red dashed line) allowing the determination of the time constant τ of current recovery from G-protein inhibition (middle panel). The arrow indicates the start of the depolarisation. Traces that allowed the measurements of RI value (in red) are also shown (bottom panel). **b** Legend as in (a) but for cells expressing $Ca_v2.1^{S218L}/\beta_4/\alpha_2\delta-1_b$ channels. **c** Time constant τ of recovery from G-protein inhibition as a function of membrane potential for $Ca_v2.1^{WT}/\beta_4/\alpha_2\delta-1_b$ channels (filled circle, $n = 13$) and $Ca_v2.1^{S218L}/\beta_4/\alpha_2\delta-1_b$ channels (open circle, $n = 13$). **d** Bar chart representation of RI values for $Ca_v2.1^{WT}/\beta_4/\alpha_2\delta-1_b$ channels (filled bars, $n = 13$) and $Ca_v2.1^{S218L}/\beta_4/\alpha_2\delta-1_b$ channels (open bars, $n = 13$) measured after 200 ms depolarization as a function of membrane potential. Data are presented as mean \pm S.E.M for n studied cells. Statistical t test: NS, non significant; *, $p \leq 0.05$; **, $p \leq 0.01$; ***, $p \leq 0.001$.

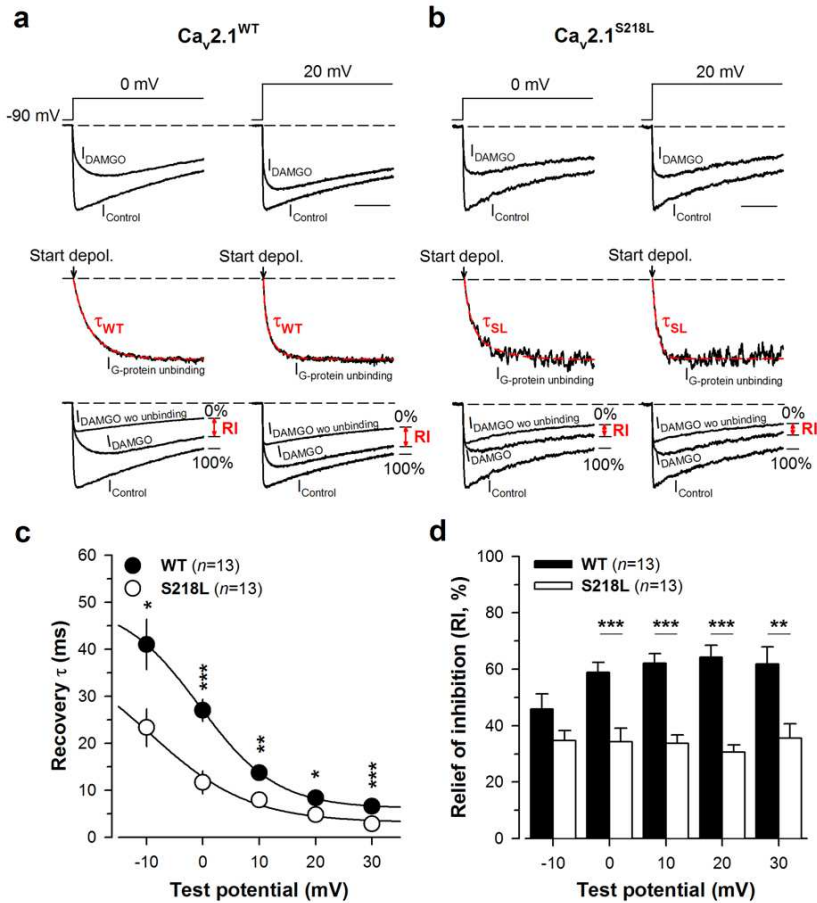


Fig. 4

Biophysical properties of $\text{Ca}_v2.1^{\text{R192Q}}$ mutated channel. **a** Average set of whole-cell current traces for $\text{Ca}_v2.1^{\text{R192Q}}/\beta_4/\alpha_2\delta-1_b$ ($n = 11$) channel obtained by 500 ms depolarization values ranging between -40 and 40 mV. Holding potential is -90 mV. **b** Average current voltage relationships for currents measured at their maximal amplitude. Inset: average half-activation potentials for wild-type (filled circles) and mutant (open circles) channels. **c** Average current time to peak values as a function of test potentials for $\text{Ca}_v2.1^{\text{R192Q}}$ mutated channel ($n = 11$). **d** Average inactivation time constants of $\text{Ca}_v2.1^{\text{R192Q}}$ channels ($n = 11$) as a function of test potential. The y-axis presents a break point for display purposes. **e** Average proportion of the inactivating component for $\text{Ca}_v2.1^{\text{R192Q}}$ channels ($n = 11$). **f** Average integrated whole cell currents for $\text{Ca}_v2.1^{\text{R192Q}}$ channels ($n = 11$) at -20 mV, -10 mV, 0 mV and 20 mV. Vertical scale: 400, 1500, 3000 and 2000 pA. ms. pF^{-1} respectively. Data are presented as mean \pm S.E.M for n studied cells. The dotted line indicates values for the $\text{Ca}_v2.1$ wild-type channel. Statistical t test: NS, non significant; *, $p \leq 0.05$; ***, $p \leq 0.001$.

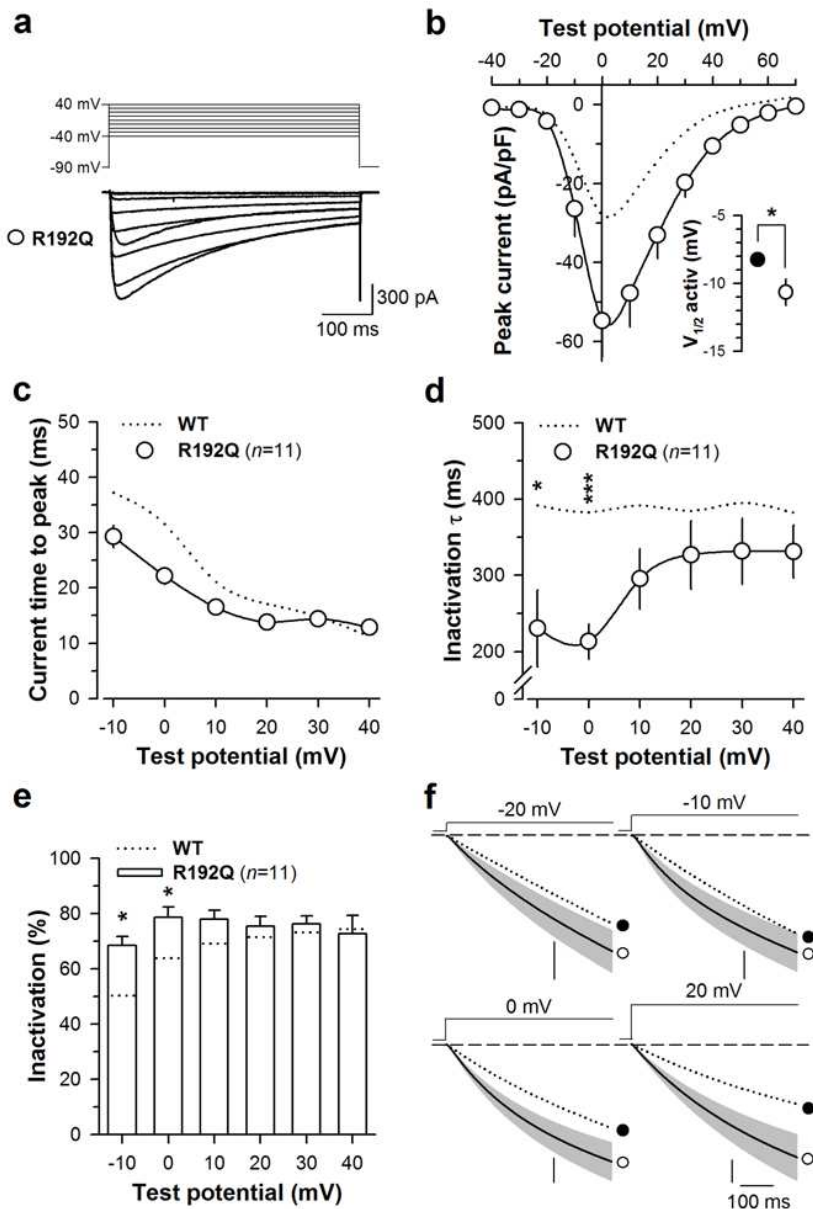


Fig. 5

The FHM-1 R192Q mutation also promotes recovery from G-protein inhibition. **a** Representative normalized current traces elicited at 0 mV (left panel) and 20 mV (right panel) before (I_{Control}) and under 10 μM DAMGO application (I_{DAMGO}) for $\text{Ca}_v2.1^{\text{R192Q}}/\beta_4/\alpha_2\delta-1_b$ channels (top panel). Corresponding traces allowing the measurement of the maximal DAMGO inhibition at the start of the depolarisation (GI_{t_0}) (bottom panel). The arrow indicates the start of the depolarisation. Scale: 50 ms. **b** Bar chart representation of GI_{t_0} for $\text{Ca}_v2.1^{\text{R192Q}}/\beta_4/\alpha_2\delta-1_b$ channels ($n = 11$) as a function of membrane potential. **c** Shift of the current time to peak induced by DAMGO application for $\text{Ca}_v2.1^{\text{R192Q}}/\beta_4/\alpha_2\delta-1_b$ channels ($n = 11$) as a function of membrane potential. **d** Normalized $I_{\text{G-protein unbinding}}$ traces at 0 mV (left panel) and 20 mV (right panel) fitted by a mono-exponential decrease (red dashed line) allowing the determination of the time constant τ of current recovery from G-protein inhibition (top panel). The arrow indicates the start of the depolarisation. Traces that allowed the measurements of RI value (in red) are also shown (bottom panel). **e** Time constant τ of recovery from G-protein inhibition as a function of membrane potential for $\text{Ca}_v2.1^{\text{R192Q}}/\beta_4/\alpha_2\delta-1_b$ channels ($n = 11$). **f** Bar chart representation of RI values for $\text{Ca}_v2.1^{\text{R192Q}}/\beta_4/\alpha_2\delta-1_b$ channels ($n = 11$) measured after 200 ms depolarization as a function of membrane potential. Data are presented as mean \pm S.E.M for n studied cells. The dotted line shows position of values for $\text{Ca}_v2.1$ wild-type channels. Statistical t test: *, $p \leq 0.05$, **, $p \leq 0.01$; ***, $p \leq 0.001$.

